

Channel Modeling for Terahertz Communications in Rain

Peian Li, Wenbo Liu, Jiacheng Liu, *Student Member, IEEE*, Da Li, Guohao Liu, Yuanshuai Lei, Jiabiao Zhao, Xiaopeng Wang, Houjun Sun, Jianjun Ma, *Member, IEEE*, John F. Federici

Abstract—Terahertz (THz) communication channels, integral to outdoor applications, are critically influenced by natural factors like rainfall. Our research focused on the nuanced effects of rain on these channels, employing an advanced rainfall emulation system. By analyzing key parameters such as rain rate, altitude-based variations in rainfall, and diverse raindrop sizes, we identified the paramount significance of the number of raindrops in the THz channel, particularly in scenarios with constant rain rates but varying drop sizes. Central to our findings is a novel model grounded in Mie scattering theory, which adeptly incorporates the variability of raindrop size distributions at different altitudes. This model has displayed strong congruence with our experimental results. In essence, our study underscores the inadequacy of solely depending on a fixed ground-based rain rate and emphasizes the imperative of calibrating distribution metrics to cater to specific environmental and operational contexts.

Index Terms—Attenuation by rain, altitude-based variation, channel modeling, raindrop size distribution, terahertz

I. INTRODUCTION

Terahertz (THz) communication offers groundbreaking potential for achieving unparalleled data rates in wireless communication systems. While enticing, the propagation characteristics of THz waves in Earth's atmosphere, notably the pronounced atmospheric losses, restrict their transmission ranges compared to conventional radio frequencies[1]. More specifically, terahertz waves are highly sensitive to water[2], meteorological conditions such as rain, snow, and fog severely impair the propagation of THz waves, necessitating a deep understanding of atmospheric attenuation to devise resilient THz communication systems[3].

Historically, initial investigations on the impact of rainfall on

This work was supported in part by the National Natural Science Foundation of China, the Science and Technology Innovation Program of Beijing Institute of Technology, the Graduate Innovative Practice Project of Tangshan Research Institute, BIT, the Talent Support Program of Beijing Institute of Technology "Special Young Scholars". (Corresponding: jianjun_ma@bit.edu.cn).

Peian Li, Wenbo Liu, Jiacheng Liu, Da Li, Guohao Liu, Yuanshuai Lei, Jiabiao Zhao are with Beijing Institute of Technology, Beijing, 100081 China
Xiaopeng Wang is with Radar Operation Control Department, Beijing, 100044 China.

Houjun Sun, Jianjun Ma are with Beijing Institute of Technology, Beijing, 100081 China and Beijing Key Laboratory of Millimeter and Terahertz Wave Technology, Beijing, 100081 China.

John F. Federici is with New Jersey Institute of Technology, New Jersey, 07102, America.

signal attenuation were primarily conducted using commercial microwave links[4,5]. However, with the surging demand for heightened data rates and expansive bandwidths, research focus has transitioned towards millimeter-wave and subsequently, terahertz communication systems[6]. Among these meteorological disturbances, the attenuation due to rainfall is particularly significant, deeply influencing THz channel behavior.

The intricacies of rainfall-induced attenuation revolve around several parameters, such as raindrop size distribution,

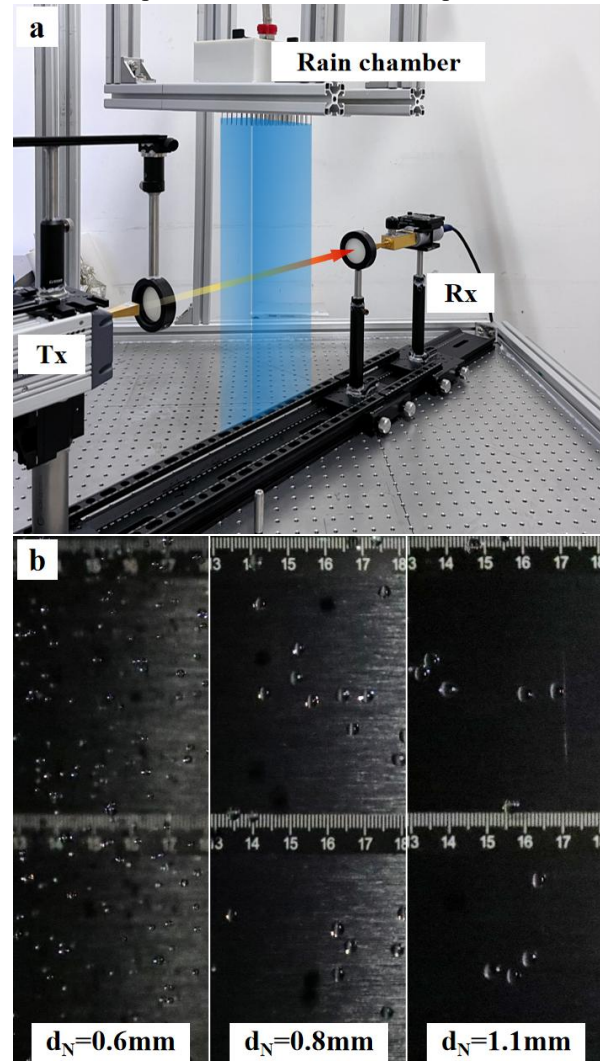


Fig. 1. (a) Schematic diagram of the rainfall attenuation measurement setup. (b) Real shot of falling raindrops at high speed shutter.

frequency of the channel, droplet morphology, and environmental temperature fluctuations. The raindrop size distribution (RSD) is frequently characterized through mathematical models, including exponential[7,8], log-normal[9], and gamma distributions[10], *etc.* By comparing observational rainfall data with these models, researchers have been able to quantify rainfall-induced attenuation using renowned models like ITU and Laws-Parsons (L-P)[11,12]. Notably, Hirata and his colleagues juxtaposed rainfall measurements at 120 GHz with various RSD models, discovering a notable alignment with the conditional Moupfouma distributions. This facilitated the computation of rainfall attenuation via the ITU and L-P models. Yet, the ITU model, while globally acclaimed, demonstrates regional limitations, often miscalculating attenuation figures in tropical climates with heavy rainfall patterns[13]. In response to such discrepancies, Budalal *et al.* introduced a modified distance factor for the ITU model, addressing the inaccuracies observed in a transmission links in Malaysia[14]. This spatial variation in rainfall attenuation primarily emerges from disparities in rain rates and RSD. Further, Wang *et al.* explored RSD attributes under distinct rainfall rates and precipitation categories, emphasizing their influence on gamma distribution parameters[15]. Even within identical regions, raindrop dimensions and densities display marked contrasts between dry and wet seasons[16].

Given the dynamic nature of rainfall, theoretical model constructions often necessitate complementary outdoor measurements. However, severe weather events like typhoons can introduce measurement inaccuracies. To mitigate wind-induced errors, Norouzian *et al.* eliminated rainfall readings during wind velocities beyond 10 m/s[17], while Weng and his colleagues devised a theoretical construct assessing wind-driven mechanical vibration impacts on attenuation[18]. Federici *et al.*, striving for a comprehensive understanding, developed weather simulation chambers to emulate varied rain conditions, incorporating image analytics to discern RSD and subsequently compute THz channel degradation through Mie scattering theory[19-21]. Beyond terrestrial transmission, rainfall attenuation becomes even more pivotal in air-to-ground communication contexts[22]. Descending droplets undergo dynamic alterations in their density, dimensions, and fall speeds due to processes like coalescence and collisions[23]. Ermis and his team formulated a backscattering model integrating particle swarm optimization with multilayered vector radiative transfer to deduce the vertical rain profile, though its efficacy waned at rain rates surpassing 12 mm/h[29]. Alarmingly, there remains a dearth of RSD altitude-centric analysis, as illustrated in Table 1, stymieing advancements in air-to-ground communication paradigms.

This work endeavors to enrich the understanding of THz channel behavior under rainfall by orchestrating controlled experiments across diverse scenarios. We meticulously examine the interplay of rain rate, droplet size, rainfall altitude, beam propagation distance, and transmission angle on channel properties. Moreover, we put forth an elevation-dependent rain

TABLE I
SUMMARY OF PUBLICATIONS ON CHANNEL MEASUREMENT AND MODELING IN RAIN

Frequency (GHz)	Distance	Scene	Remarks	Ref.
8-38	0.5-27 km	Outdoor	Non-linear tomographic model, commercial microwave links	[3]
120	400 m	Outdoor	Moupfouma distribution, ITU and Laws and Parsons model	[11]
100-1000	4 m	Indoor	Mie scattering model, Gaussian distribution, rain emulation chamber	[19]
625	3 m	Indoor	Compred with infrared links, weather emulating chamber	[20]
14-39	1.5-7 km	Outdoor	Machine learning employed	[4]
25-75	100-300 m	Outdoor	Distance and increment factors	[14]
77-300	160 m	Outdoor	Corrected raindrop size distribution mode	[17]
75-400	1-12 km	Outdoor	Violent rain, strong winds	[18]
140-675	4 m	Indoor	QAM modulated data stream, Mie scattering theory, measured size distribution	[21]
25-77	36-200 m	Outdoor	Long term attenuation, raindrops induced scattering, ITU-R P.530-18 model, rain mixed with snow	[27]
130-150	70 m	Outdoor	Rain attenuation, snow-induced delay spread, multipath profile	[28]
13-35	4-5 km	Outdoor	Particle swarm optimization, vector radiative transfer, backscattering model, vertical profile of rain	[29]

attenuation model synergized with Mie scattering theory, elucidating the intricate interactions of the aforementioned parameters.

The subsequent sections of this paper are structured as follows: Section 2 delineates the rainfall measurement apparatus and showcases high-resolution imagery of droplets under varying conditions. Section 3 deliberates on the influence of raindrop size and concentration on attenuation. Section 4 discusses the impact of rainfall altitudes on attenuation, introducing an altitude-adjusted RSD attenuation model. Section 5 engages in air-to-ground communication simulations to validate the revised RSD model's applicability. Section 6 documents outdoor rainfall measurements, and Section 7 encapsulates our discoveries and conclusions.

II. EXPERIMENTAL SETUP

The experimental framework developed for this study combines a state-of-the-art terahertz (THz) transceiver system (same as that in reference [21]) with a meticulously designed rain generation module, as illustrated in Fig. 1(a). Central to this apparatus is the rain chamber, a polyethylene (PE)

constructed module with dimensions of $17\text{cm} \times 11\text{cm} \times 5\text{cm}$ (length \times width \times height). The chamber integrates a water inlet (with an inner diameter, $d = 3\text{ mm}$) on one side and 98 water outlets (each having an inner diameter, $d = 2\text{ mm}$) on the opposite end. For precise control over raindrop dimensions, disposable medical needles are affixed to these outlets. The choice of needle, specifically its inner diameter, directly influences the size of the raindrop produced. Within the chamber, the outlets cover an approximate area of $13\text{cm} \times 6\text{cm}$ (length \times width), systematically arranged in a 14×7 grid pattern with a consistent 1 cm inter-outlet spacing.

Auxiliary components of this apparatus include a pressure pump and a flow meter, responsible for adjusting and maintaining the desired rainfall intensity. The entire rain generation system is sturdily anchored onto an optical platform using iron frames. The chamber's position can be modified by tweaking the iron frame's alignment, allowing for varied rain angles and orientations. Moreover, to adjust the THz transceiver's relative position, a markable pulley system is employed. The THz transceiver system plays a pivotal role in assessing rain-induced attenuation. During the experimentation phase, the system's position was varied in accordance to the desired measurement parameters by utilizing the aforementioned pulley system.

To comprehensively study rain-induced attenuation phenomena, four distinct rainfall intensities were set: 733 mm/hr , 2786 mm/hr , 8065 mm/hr , and 14296 mm/hr . It is noteworthy that such elevated rain rates are uncharacteristic of natural rainfall patterns but were deemed necessary for our laboratory setup due to the restricted channel distance ($< 1\text{m}$). For the purpose of this study, emphasis was placed on the two higher rainfall intensities.

In conjunction with rainfall intensity, raindrop size was another critical parameter. Fig. 1(b) offers a visual representation of raindrops under a rain rate of 8065 mm/hr , corresponding to needle inner diameters of 0.6 mm , 0.8 mm , and 1.1 mm . It was observed that, while maintaining a constant rainfall intensity, there exists an inverse relationship between the raindrop size and their total count.

In this work, all experiments were conducted under controlled laboratory conditions. The ambient temperature and humidity levels, influencing the THz propagation path, were meticulously monitored. Variations in these environmental conditions were minimized and neglected across all tests.

III. SIGNAL ANALYSIS BASED ON RAINDROP SIZE

Raindrops in the atmosphere typically exhibit sizes ranging from 0.1mm to 8mm . It is crucial to note that larger raindrops, due to the overpowering effects of aerodynamic forces compared to cohesive surface tension, do not sustain for extended durations in the atmosphere. The raindrop size distribution (RSD) provides a metric for the number of drops per unit volume for each interval of drop diameter, while the rain rate offers an aggregated measure of rainfall depth over time. Although most rainfall phenomena correlate with the rain rate to some extent, it is conventional to represent RSD as a function of this rate when designing empirical models.

However, it's imperative to understand that the density of raindrops per cubic meter can show considerable disparities, from a sparse few at the forefront of a convective rainfall to possibly surpassing $10,000$ in dense regions[23]. Thus, for accurate electromagnetic modeling, an in-depth analysis of RSD under diverse conditions is crucial.

In this work, we initiated experiments where terahertz channels passed through a rain chamber maintained at a consistent rain rate of 8065 mm/hr . The variable in these tests was the inner diameter of the needle responsible for controlling raindrop size. As delineated in Section 2, this inner diameter plays a pivotal role in determining both the size and count of raindrops. However, due to minor variations in the chamber's water pressure, droplet sizes exhibited a deviation of about $\pm 0.5\text{mm}$ across separate trials. Consequently, our focus shifted to assessing the nuances of rainfall attenuation for a constant rain rate while factoring in different raindrop sizes.

Fig. 2(a) offers a visualization of how rainfall attenuation varies with frequency. Interestingly, raindrops produced from 0.6mm needles, despite their smaller size, resulted in the most significant attenuation due to their abundance. This observation aligns with findings from reference[23], which emphasizes that terahertz channel degradation can differ substantially even if

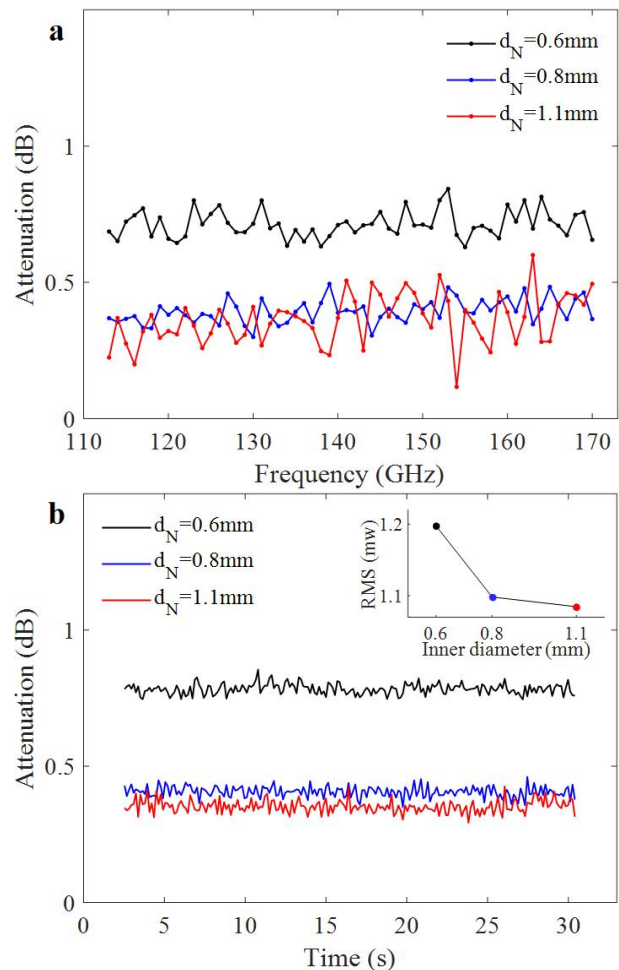


Fig. 2. (a) Variation of rainfall attenuation with respect to operating frequency under different raindrop size distributions. (b) Rainfall attenuation on wireless channels operating at 140GHz under a rain rate of 8065 mm/hr during 28s . Insert: Root mean square (RMS) of rainfall attenuation.

rain rates are identical – the distinction stems from the variation in raindrop sizes. Raindrops generated from 0.8mm and 1.1mm needles, although different in count and size, demonstrated similar attenuation patterns. Further, Fig. 2(b) captures the variability in rainfall attenuation experienced by a 140GHz channel over a duration of 28 seconds. The signal data, sampled at intervals of 0.14 seconds, is represented by a curated selection of 200 data points in the plot. To comprehend the influence of raindrop size on signal consistency, we calculated the root mean square (RMS) of the rainfall attenuation across the observed duration. The inset plot lucidly suggests that an augmented raindrop count in the beam's path tends to amplify signal inconsistencies. Such behavior can be ascribed to the heightened variability in the instantaneous raindrop count, amplifying the random scattering effects, a phenomenon supported by discussions in Section 4.

IV. HEIGHT-INDUCED RDSV VARIATION

In previous observations, a prominent transformation was discerned in the distribution of raindrops as a function of altitude[30]. Several meteorological factors, encompassing cumulonimbus cloud formations, alterations in atmospheric pressure, and variability in wind speeds, contribute to this phenomenon, which affects the raindrop intensity and distribution with changing altitude. It's worth noting that as raindrops fall, they encounter varying gravitational forces and aerodynamic drag based on their sizes. This dynamic interplay can lead to collisions leading to coalescence or fragmentation due to mechanical disruptions, altering the raindrop's

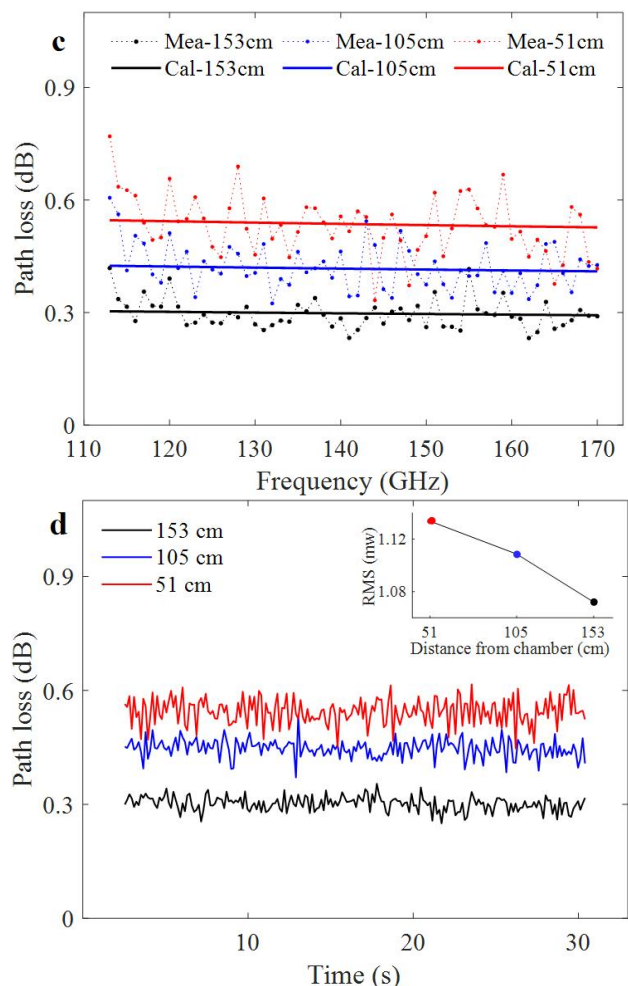
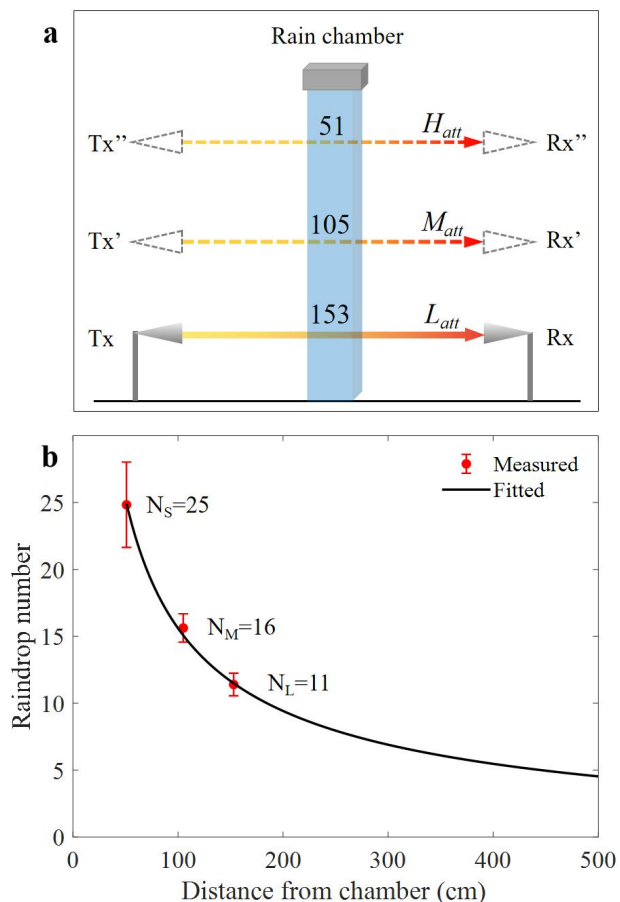


Fig. 3. (a) Illustration detailing signal propagation across varying heights within the rain-affected zone (specific beam distances from the chamber are 51 cm, 105 cm, and 153 cm). (b) Instantaneous fluctuations in the count of raindrops traversing the channel beam at distinct altitudes. (c) Comparative data on empirically observed and theoretically computed rain attenuation, stratified by operating frequencies and altitudes. (d) Analysis of attenuation in wireless channels at 140GHz, subjected to a rain intensity of 8065 mm/hr over a span of 28 seconds. Inset: Root Mean Square (RMS) analysis of rainfall-induced attenuation across the three examined heights (51cm, 105cm, 153cm).

microphysical attributes[23]. Consequently, these changes directly influence the raindrop size distribution at distinct heights.

The experimental setup, portrayed in Fig. 3(a), was meticulously designed to gauge rainfall attenuation across three distinct heights: 51 cm, 105 cm, and 153 cm from the rain chamber, labeled as H_{att} , M_{att} , and L_{att} , respectively. As the height of the beam shifts, the count of raindrops intersecting it varies correspondingly, which equivalents to altitude variation of the terahertz channels. A high-speed camera with a shutter speed of 1/8000 seconds was deployed to capture these dynamics by taking numerous snapshots, registering instantaneous variations in raindrop counts within the beam's path.

Fig. 3(b) delineates the raindrop counts at the aforementioned heights at a given moment, flowing from 0.8mm needles. Observationally, at 51cm from the rain chamber, about 25 raindrops intersect the beam. This number dwindles to approximately 16 at 105 cm, and further to around

11 at 153 cm. It's intriguing to observe that as the beam's distance from the chamber augments, the variability in raindrop counts begins to attenuate, suggesting that after a specific range, the raindrop distribution reaches a form of stability. The black fitting curve in Fig. 3 (b) shows this trend, following a power function

$$N_{rd} = 335.4 \times D^{-0.646} - 1.525 \quad (1)$$

where, D is the rainfall distance from the rain chamber, N_{rd} represents the number of raindrops at the distance D . Reference [23] mentions that the mass flux of raindrops is proportional to the final velocity. As raindrops fall, they collide and merge with one another, leading to an increase in their size. Additionally, due to air resistance, the velocity of a raindrop will eventually stabilize and reach what is known as its terminal velocity [24-26]. Based on this understanding, we can infer that in the region where the terminal velocity is stable, the size of the raindrops would also stabilize and hence, the number of raindrops would remain relatively constant. Therefore, in Fig. 2(b), we have utilized an exponential function to fit the data, because the initial part of this function aligns with our measured data, and it approaches a stable value in the latter half.

While rainfall rate offers a quantitative measure of ground-level rain intensity, it falls short in encapsulating the intricate microphysical characteristics of individual raindrops. To bridge this gap, we incorporated empirical mathematical models grounded on observed size spectra to emulate natural raindrop distributions. The raindrops generated by our setup predominantly conformed to an exponential distribution, described as:

$$N(D) = N_0 \exp(-\Lambda D) \quad (2)$$

where, $N(D)$ is the number density of raindrops with a diameter D per unit volume, N_0 represents the number of raindrops within the radius $r+dr$ per unit volume, and Λ characterizes the distribution's shape. Maintaining the premise that raindrops at various altitudes, but from a uniform source, follow a consistent distribution pattern, we modified the N_0 parameter according to our measurements. Subsequently, using the Mie scattering theory, we computed the rainfall attenuation. Our model's predictions exhibited remarkable concordance with empirical data, as portrayed in Fig. 3(c).

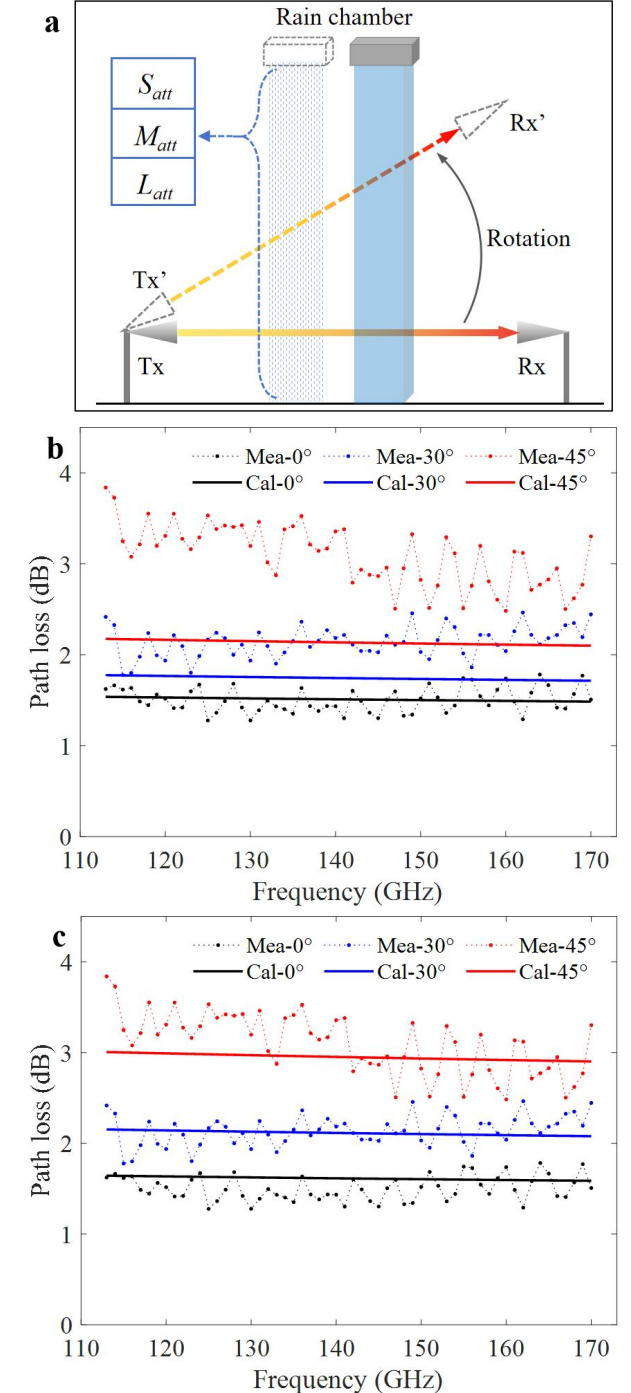
Following the methodology delineated in Section 3, signal perturbations at 140GHz were monitored over a designated period, with their root mean square (RMS) subsequently computed. Fig.3(d) accentuates that as the beam approaches the rain chamber, there's a noticeable upsurge in rainfall attenuation, culminating in heightened signal perturbations. In situations where raindrop sizes remain relatively constant, the count of raindrops within the beam and the inherent randomness they introduce predominantly dictate signal stability.

V. HEIGHT-INDUCED CHANNEL DEGRADATION

Communication services that operate from air to ground, such as aviation communication systems, meteorological observation, and remote data sensing, necessitate both high

reliability and expansive bandwidth. Among the plethora of variables affecting these systems, the alteration of raindrop size distribution due to altitude shifts stands out as particularly significant[31].

To empirically validate the implications of this phenomenon,



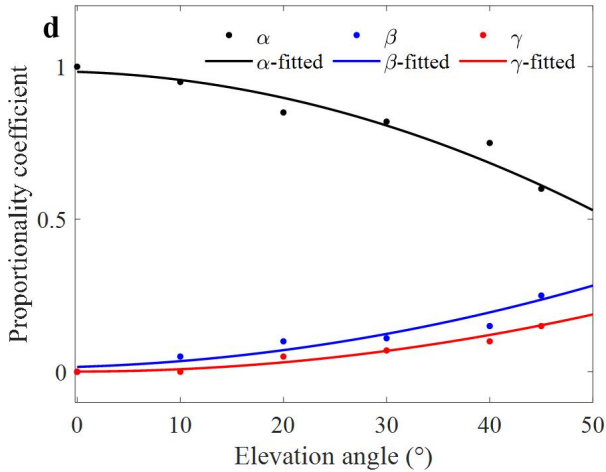


Fig. 4. (a) Illustration of signal propagation across varied elevation angles, spanning 0° to 45° . (b) Measured and predicted results in the absence of altitude-induced raindrop size alterations. (c) Measured and computed outcomes considering the additional attenuation introduced by altitude (height) shifts. The color-coding in the graph aligns with that in Fig. 4(b). (d) Computed and fitted metrics for the three proportionality constants. Point values signify computed data, whereas continuous lines represent the adjusted values. The black data set (α / α -fitted) is indicative of the proportionality factor when the rain chamber stands at a distance of 153cm from the beam, blue data (β / β -fitted) pertains to a height of 105cm, and red data (γ / γ -fitted) is associated with a 51cm elevation.

our team carried out controlled laboratory simulations emulating realistic air-to-ground communication situations. As demonstrated in Fig. 4(a), we established a fixed transmitter-receiver (Tx-Rx) pair, ensuring uniformity in signal trajectory and transmission range. Concurrently, we adjusted the rain chamber's horizontal placement to emulate the rotation of the entire apparatus, thereby ensuring that the distance between the rain-introduced region and the receiving antenna (Rx) remained unchanged. With an increase in the elevation angle, the primary contributors to signal attenuation were identified to be: the variations in the height of the beam and its trajectory within the rain-affected area.

Our initial focus lay on assessing the rain-induced attenuation based on the alteration in path due to shifting elevation angles. This is portrayed in Fig. 4(b). While the findings clearly indicate that an elongation in path length leads to enhanced attenuation, a more intricate interpretation of the acquired data is necessary due to significant observed variations. Incorporating our updated model of raindrop size distribution, which now factored in height-induced changes, we used three nomenclatures: L_{att} , M_{att} , and H_{att} , to represent the rainfall attenuation at distances of 153cm, 105cm, and 51cm from the beam to the rain zone, respectively. As visualized in Fig. 4(c), at an elevation angle of 0° , where the beam is co-planar with the ground, only L_{att} is applicable. Yet, with the rotation of the Tx-Rx pair as indicated in Fig. 4(a), both M_{att} and H_{att} values show a noticeable augmentation, while L_{att} exhibits a decline.

For a more granular understanding of altitude-dependent attenuation fluctuations, we incorporated a mathematical equation:

$$PL = \frac{H_m}{H_a} (\alpha \cdot L_{att} + \beta \cdot M_{att} + \gamma \cdot H_{att}) \quad (3)$$

where, PL signifies the path loss of the signal. H_m represents the apex distance from the rain chamber to the beam, set at 153cm in our study, whereas H_a accounts for the real-time altitude during signal propagation, encompassing deviations from our base model. We divided the altitude range into three distinct sections, with each segment presumed to have a consistent signal attenuation corresponding to L_{att} , M_{att} and H_{att} . The proportionality constants α , β and γ pertain to these divisions, symbolizing the fractions of the signal traversing the rain-affected region at diverse elevation angles. While our current model operates on these three divisions, subsequent inquiries could introduce more nuanced segmentation tailored to specific use-cases, enhancing the accuracy of this model. Fig. 4(d) pictorially delineates the computed and adapted values for these proportion factors. As elevation augments, the influence of M_{att} and H_{att} strengthens, contrasted by a decrease in L_{att} 's contribution. This trend is congruent with field observations[23].

VI. OUTDOOR EXPERIMENTAL VALIDATION

A persistent challenge in understanding rain-induced attenuation in communication channels lies in the limitations of empirical models, which predominantly hinge on ground-based rainfall rate measurements. Such models might not fully account for the nuanced influence of factors such as spatial structures, altitude-related changes in raindrop size distribution (RSD), and varied climatic conditions. Recognizing this gap, this work introduces a RSD-based correction model tailored to adapt to altitude-induced variations.

To put our proposed model to the test and establish its viability, we embarked on a systematic outdoor experimentation phase. The experimental setup was strategically located in the Liangxiang campus of the Beijing Institute of Technology. This location provided us with a 41.4-meter-long communication channel nestled between two infrastructural edifices, as vividly illustrated in Fig. 5(a). Our methodology was comprehensive: measuring link performance not only under rainy conditions but also when the skies were clear, offering a benchmark comparison.

The experiment was serendipitously timed with the onset of Typhoon DuSuri, a circumstance that enriched our dataset with a wide spectrum of rainfall rates. Systematic data acquisition was paramount: signal data was meticulously logged at one-minute intervals spanning a duration of 90 minutes. Simultaneously, rain rate recordings were taken every ten minutes. A scrutiny of Fig. 5(b) showcases the distribution of the captured rain rates, with pronounced concentrations at 6.8 mm/hr, 7.6 mm/hr, 15.3 mm/hr, and 30.6 mm/hr.

Building upon the widely-accepted exponential distribution model, we incorporated refinements by adjusting both its quantity and shape parameters in accordance with the real-time observed rain rates. To ascertain rainfall attenuation, the Mie scattering theory was employed, and the subsequent results were elegantly encapsulated in the calculation curve represented by the yellow line in Fig. 5(b). Encouragingly, our computational findings demonstrated commendable alignment

with the empirically measured values, thereby reinforcing the credibility and utility of our proposed RDSD correction model.

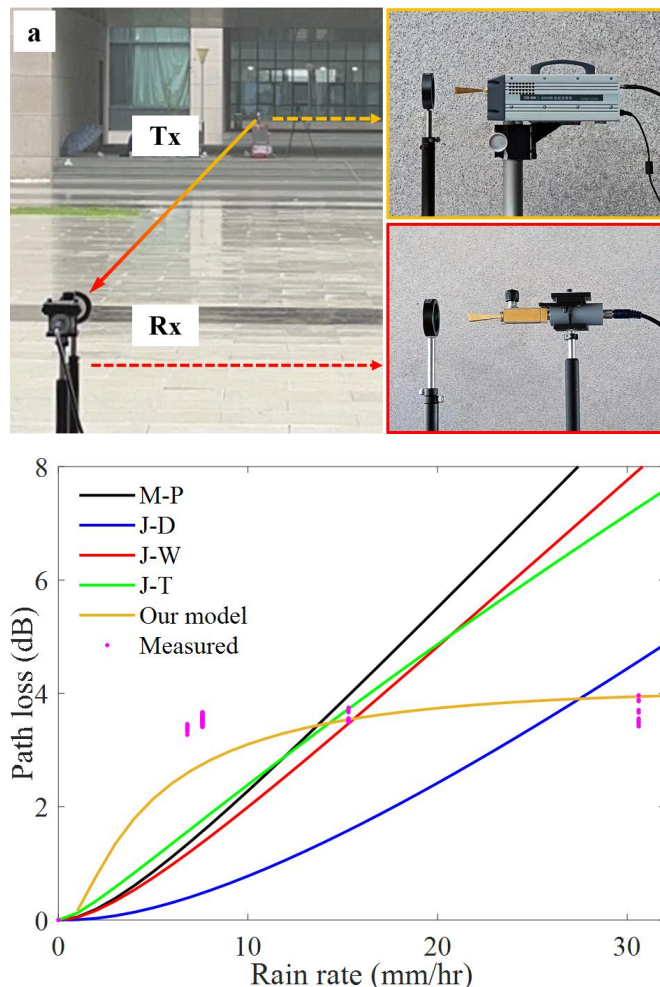


Fig. 5. (a) schematic representation of the outdoor setup designed to gauge rainfall attenuation experienced by a 140GHz channel. (b) Calculations from prevailing models (M-P, J-D, J-W, J-T) with those from our innovative RDSD correction model, juxtaposed with real-time measurements spanning diverse rainfall intensities.

VII. CONCLUSION

This work delves deep into how rain impacts terahertz communication channels. Utilizing a controlled rain emulation system, we investigated various parameters like rain rate, height, and raindrop size. Our results confirmed that, with a consistent rain rate, the raindrop size distribution (RDSD) in the THz channel is the key factor determining signal attenuation. Moreover, we introduced a new RDSD model considering varying heights (altitude). This model, combined with Mie scattering theory, effectively simulates rainfall attenuation and matches our experimental results.

Practically, our findings indicate that solely relying on ground-based rain rates might be insufficient. Instead, adjusting distribution factors based on specific situations is necessary for optimal communication system performance.

ACKNOWLEDGMENT

We appreciate the help from Beijing Institute of Technology for providing us with the experimental site for rainfall environment channel measurement.

REFERENCES

- [1] R. Wang, Y. Mei, X. Meng, and J. Ma, "Secrecy performance of terahertz wireless links in rain and snow," *Nano Communication Networks*, vol. 28, p. 100350, 2021.
- [2] J. Lou et al. "Calibration-free, high-precision, and robust terahertz ultrafast metasurfaces for monitoring gastric cancers", Proceedings of the National Academy of Sciences of the United States of America, vol. 119, no. 43, pp. e2209218119, 2022.
- [3] A. Zinevich, P. Alpert, and H. Messer, "Estimation of rainfall fields using commercial microwave communication networks of variable density," *Advances in water resources*, vol. 31, no. 11, pp. 1470-1480, 2008.
- [4] D. Jacoby, J. Ostrometzky, and H. Messer, "Short-term prediction of the attenuation in a commercial microwave link using LSTM-based RNN," in 2020 28th European Signal Processing Conference (EUSIPCO), 2021: IEEE, pp. 1628-1632.
- [5] E. Alozie et al., "A review on rain signal attenuation modeling, analysis and validation techniques: Advances, challenges and future direction," *Sustainability*, vol. 14, no. 18, p. 11744, 2022.
- [6] A. M. Al-Saman, M. Cheffena, M. Mohamed, M. H. Azmi, and Y. Ai, "Statistical analysis of rain at millimeter waves in tropical area," *IEEE Access*, vol. 8, pp. 51044-51061, 2020.
- [7] J. S. Marshall and W. M. K. Palmer, "The distribution of raindrops with size," *Journal of Atmospheric Sciences*, vol. 5, no. 4, pp. 165-166, 1948.
- [8] G. Zhang, M. Xue, Q. Cao, and D. Dawson, "Diagnosing the intercept parameter for exponential raindrop size distribution based on video disdrometer observations: Model development," *Journal of applied meteorology and climatology*, vol. 47, no. 11, pp. 2983-2992, 2008.
- [9] D. A. de Wolf, "On the Laws-Parsons distribution of raindrop sizes," *Radio Science*, vol. 36, no. 4, pp. 639-642, 2001.
- [10] G. O. Ajayi and R. L. Olsen, "Modeling of a tropical raindrop size distribution for microwave and millimeter wave applications," *Radio Science*, vol. 20, no. 02, pp. 193-202, 1985.
- [11] A. Hirata et al., "Effect of rain attenuation for a 10-Gb/s 120-GHz-band millimeter-wave wireless link," *IEEE transactions on microwave theory and techniques*, vol. 57, no. 12, pp. 3099-3105, 2009.
- [12] R. Series, "Propagation data and prediction methods required for the design of terrestrial line-of-sight systems," *Recommendation ITU-R*, pp. 530-12, 2015.
- [13] O. Darley, A. I. Yussuff, and A. A. Adenowo, "Investigation into rain attenuation prediction models at locations in lagos using remote sensing," *FUOYE Journal of Engineering and Technology*, vol. 6, no. 2, pp. 19-24, 2021.
- [14] A. A. H. Budalal, M. R. Islam, K. Abdullah, and T. A. Rahman, "Modification of Distance Factor in Rain Attenuation Prediction for Short-Range Millimeter-Wave Links," *IEEE ANTENNAS AND WIRELESS PROPAGATION LETTERS*, vol. 19, no. 6, p. 1027, 2020.
- [15] G. Wang, R. Li, J. Sun, X. Xu, R. Zhou, and L. Liu, "Comparative analysis of the characteristics of rainy season raindrop size distributions in two typical regions of the Tibetan Plateau," *Advances in Atmospheric Sciences*, vol. 39, no. 7, pp. 1062-1078, 2022.
- [16] R. Lai et al., "Raindrop size distribution characteristic differences during the dry and wet seasons in South China," *Atmospheric Research*, vol. 266, p. 105947, 2022.
- [17] F. Norouzian et al., "Rain attenuation at millimeter wave and low-THz frequencies," *IEEE Transactions on Antennas and Propagation*, vol. 68, no. 1, pp. 421-431, 2019.
- [18] Z.-K. Weng et al., "Millimeter-wave and terahertz fixed wireless link budget evaluation for extreme weather conditions," *IEEE Access*, vol. 9, pp. 163476-163491, 2021.

- [19] J. Ma, F. Vorrius, L. Lamb, L. Moeller, and J. F. Federici, "Comparison of experimental and theoretical determined terahertz attenuation in controlled rain," *Journal of Infrared, Millimeter, and Terahertz Waves*, vol. 36, pp. 1195-1202, 2015.
- [20] J. Ma, F. Vorrius, L. Lamb, L. Moeller, and J. F. Federici, "Experimental comparison of terahertz and infrared signaling in laboratory-controlled rain," *Journal of Infrared, Millimeter, and Terahertz Waves*, vol. 36, pp. 856-865, 2015.
- [21] P. Li et al., "Performance degradation of terahertz channels in emulated rain," *Nano Communication Networks*, vol. 35, p. 100431, 2023.
- [22] V. Doborshchuk, V. Begishev, and K. Samouylov, "Propagation Model for Ground-to-Aircraft Communications in the Terahertz Band with Cloud Impairments," *Energies*, vol. 15, no. 21, p. 8022, 2022.
- [23] G. Zhang, "Dual polarization radar meteorology," China Meteorological Press, 2018.
- [24] D. Atlas, C. W. Ulbrich, "Path-and area-integrated rainfall measurement by microwave attenuation in the 1-3 cm band," *Journal of Applied Meteorology*, vol. 16, pp. 1322-1331, 1977.
- [25] D. Atlas, R. C. Srivastava, and R. S. Sekhon, "Doppler radar characteristics of precipitation at vertical incidence," *Reviews of Geophysics*, vol. 11, pp. 1-35, 1973.
- [26] E. A. Brandes, G. Zhang, and J. Vivekanandan, "Experiments in rainfall estimation with a polarimetric radar in a subtropical environment," *Journal of Applied Meteorology*, vol. 41, pp. 674-685, 2002.
- [27] O. Zahid and S. Salous, "Long-term rain attenuation measurement for short-range mmWave fixed link using DSD and ITU-R prediction models," *Radio Science*, vol. 57, no. 4, pp. 1-21, 2022.
- [28] P. Sen et al., "Terahertz communications can work in rain and snow: Impact of adverse weather conditions on channels at 140 GHz," in *Proceedings of the 6th ACM Workshop on Millimeter-Wave and Terahertz Networks and Sensing Systems*, 2022, pp. 13-18.
- [29] S. Ermis and E. Yigit, "Estimation of rain parameters for microwave backscattering model using PSO," *Atmospheric Research*, vol. 288, p. 106720, 2023.
- [30] H. Zheng, Y. Zhang, L. Zhang, H. Lei, and Z. Wu, "Precipitation microphysical processes in the inner rainband of tropical cyclone Kajiki (2019) over the South China Sea revealed by polarimetric radar," *Advances in Atmospheric Sciences*, vol. 38, pp. 65-80, 2021.
- [31] A. M. Shalaby and N. S. Othman, "The effect of rainfall on the uav placement for 5g spectrum in malaysia," *Electronics*, vol. 11, no. 5, p. 681, 2022.